

# Large deformed structures in $Ne - S$ nuclei near neutron drip-line

S.K. Patra and C.R. Praharaj

*Institute of Physics, Sachivalaya Marg, Bhubaneswar-751 005, India*

(Dated: September 16, 2021)

The structure of Ne, Na, Mg, Al, Si and S nuclei near the neutron drip-line region is investigated in the framework of relativistic meanfield (RMF) and non-relativistic Skyrme Hartree-Fock formalisms. The drip-line of these nuclei are pointed out. We analysed the large deformation structures and many of these neutron rich nuclei are quite deformed. New magic number are seen for these deformed nuclei.

PACS numbers: 21.10.-k, 21.10.dr, 21.10.Ft, 21.30.-x, 24.10.-1, 24.10.Jv

## I. INTRODUCTION

The structure of light nuclei near the neutron drip-line is very interesting for a good number of exotic phenomena. Nuclei in this region are very different in collectivity and clustering features than the stable counterpart in the nuclear chart. For example, the neutron magicity is lost for the  $N=8$  nucleus for  $^{12}\text{Be}$  [1] and  $N=20$  for  $^{32}\text{Mg}$  [2]. The discovery of large collectivity of  $^{34}\text{Mg}$  by Iwasaki et al. [3] is another example of such properties. The deformed structures and core excitations of Mg and neighboring nuclei and location of drip-line in this mass region is an important matter [4]. On the other hand, the appearance of  $N=16$  magic number for  $^{24}\text{O}$  is well established [5]. The discovery of the two isotopes  $^{40}\text{Mg}$  and  $^{42}\text{Al}$ , once predicted to be drip-line nuclei [6, 7] gives indication that the neutron drip-line is located towards the heavier mass region. The existence of neutron halo in  $^{11}\text{Li}$  is well established and the possibility of proton halo in  $^8\text{B}$  and the neutron halo in  $^{14}\text{Be}$  and  $^{17}\text{B}$  are very interesting phenomena for the drip-line nuclei. In addition to these above exciting properties, the cluster structure of entire light mass nuclei and the skin formation in neutron-drip nuclei provide us features for the study of light mass drip-line nuclei. Also, the exotic neutron drip-line nuclei play a role in many astrophysical studies. In this paper, our aim is to study the neutron drip-line for Ne-S isotopic chain in the frame-work of a relativistic mean field (RMF) and non-relativistic Skyrme Hartree-Fock formalism and analyse the large deformation of these isotopes.

The paper is organised as follows: The relativistic and non-relativistic mean field formalisms are described very briefly in Section II. The results obtained from the relativistic mean field (RMF) and Skyrme-Hartree-Fock (SHF) formalisms, and a discussion of these results, are presented in Section III. Finally summary and concluding remarks are given in Section IV.

## II. THEORETICAL FRAMEWORK

Mean field methods have been widely used in the study of binding energies and other properties of nuclei [8, 9]. Although the older version of the SHF and RMF models have some limitation to reproduce some of the observables, the recent formalisms are quite efficient to predict the bulk properties of nuclei not only near the stability valley, but also for

the nuclei near the proton and neutron drip-lines. We use here two of the successful mean field models [8, 10–16] (Skyrme Hartree-Fock and the Relativistic Mean Field) to learn about the properties of drip-line nuclei  $Ne - S$ .

### A. The Skyrme Hartree-Fock (SHF) Method

There are many known parametrizations of Skyrme interaction which reproduce the experimental data for ground-state properties of finite nuclei and for the observables of infinite nuclear matter at saturation densities, giving more or less comparable agreements with the experimental or expected empirical data. The general form of the Skyrme effective interaction, used in the mean-field models, can be expressed as a density functional  $\mathcal{H}$  [10, 11], given as a function of some empirical parameters, as

$$\mathcal{H} = \mathcal{K} + \mathcal{H}_0 + \mathcal{H}_3 + \mathcal{H}_{eff} + \dots \quad (1)$$

where  $\mathcal{K}$  is the kinetic energy term,  $\mathcal{H}_0$  the zero range,  $\mathcal{H}_3$  the density dependent and  $\mathcal{H}_{eff}$  the effective-mass dependent terms, which are relevant for calculating the properties of nuclear matter. These are functions of 9 parameters  $t_i$ ,  $x_i$  ( $i = 0, 1, 2, 3$ ) and  $\eta$ , and are given as

$$\mathcal{H}_0 = \frac{1}{4}t_0 [(2 + x_0)\rho^2 - (2x_0 + 1)(\rho_p^2 + \rho_n^2)], \quad (2)$$

$$\mathcal{H}_3 = \frac{1}{24}t_3\rho^\eta [(2 + x_3)\rho^2 - (2x_3 + 1)(\rho_p^2 + \rho_n^2)], \quad (3)$$

$$\begin{aligned} \mathcal{H}_{eff} = & \frac{1}{8} [t_1(2 + x_1) + t_2(2 + x_2)] \tau \rho \\ & + \frac{1}{8} [t_2(2x_2 + 1) - t_1(2x_1 + 1)] (\tau_p \rho_p + \tau_n \rho_n). \end{aligned} \quad (4)$$

The kinetic energy  $\mathcal{K} = \frac{\hbar^2}{2m}\tau$ , a form used in the Fermi gas model for non-interacting fermions. The other terms, representing the surface contributions of a finite nucleus with  $b_4$

and  $b'_4$  as additional parameters, are

$$\begin{aligned} \mathcal{H}_{S\rho} = & \frac{1}{16} \left[ 3t_1(1 + \frac{1}{2}x_1) - t_2(1 + \frac{1}{2}x_2) \right] (\vec{\nabla}\rho)^2 \\ & - \frac{1}{16} \left[ 3t_1(x_1 + \frac{1}{2}) + t_2(x_2 + \frac{1}{2}) \right] \\ & \times \left[ (\vec{\nabla}\rho_n)^2 + (\vec{\nabla}\rho_p)^2 \right], \text{ and} \end{aligned} \quad (5)$$

$$\mathcal{H}_{S\vec{J}} = -\frac{1}{2} \left[ b_4\rho\vec{\nabla} \cdot \vec{J} + b'_4(\rho_n\vec{\nabla} \cdot \vec{J}_n + \rho_p\vec{\nabla} \cdot \vec{J}_p) \right]. \quad (6)$$

Here, the total nucleon number density  $\rho = \rho_n + \rho_p$ , the kinetic energy density  $\tau = \tau_n + \tau_p$ , and the spin-orbit density  $\vec{J} = \vec{J}_n + \vec{J}_p$ . The subscripts  $n$  and  $p$  refer to neutron and proton, respectively, and  $m$  is the nucleon mass. The  $\vec{J}_q = 0$ ,  $q = n$  or  $p$ , for spin-saturated nuclei, i.e., for nuclei with major oscillator shells completely filled. The total binding energy (BE) of a nucleus is the integral of the density functional  $\mathcal{H}$ .

At least eighty-seven parametrizations of the Skyrme interaction are published since 1972 [12] where  $b_4 = b'_4 = W_0$ , we have used here the Skyrme SkI4 set with  $b_4 \neq b'_4$  [13]. This parameter set is designed for considerations of proper spin-orbit interaction in finite nuclei, related to the isotope shifts in Pb region and is better suited for the study of exotic nuclei. Several more recent Skyrme parameters such as SLy1-10, SkX, SkI5 and SkI6 are obtained by fitting the Hartree-Fock (HF) results with experimental data for nuclei starting from the valley of stability to neutron and proton drip-lines [10, 13, 14, 17].

## B. The Relativistic Mean Field (RMF) Method

The relativistic mean field approach is well-known and the theory is well documented [15, 16]. Here we start with the relativistic Lagrangian density for a nucleon-meson many-body system, as

$$\begin{aligned} \mathcal{L} = & \bar{\psi}_i \{ i\gamma^\mu \partial_\mu - M \} \psi_i + \frac{1}{2} \partial^\mu \sigma \partial_\mu \sigma - \frac{1}{2} m_\sigma^2 \sigma^2 \\ & - \frac{1}{3} g_2 \sigma^3 - \frac{1}{4} g_3 \sigma^4 - g_s \bar{\psi}_i \psi_i \sigma - \frac{1}{4} \Omega^{\mu\nu} \Omega_{\mu\nu} \\ & + \frac{1}{2} m_w^2 V^\mu V_\mu + \frac{1}{4} c_3 (V_\mu V^\mu)^2 - g_w \bar{\psi}_i \gamma^\mu \psi_i V_\mu \\ & - \frac{1}{4} \vec{B}^{\mu\nu} \cdot \vec{B}_{\mu\nu} + \frac{1}{2} m_\rho^2 \vec{R}^\mu \cdot \vec{R}_\mu - g_\rho \bar{\psi}_i \gamma^\mu \vec{\tau} \psi_i \cdot \vec{R}^\mu \\ & - \frac{1}{4} F^{\mu\nu} F_{\mu\nu} - e \bar{\psi}_i \gamma^\mu \frac{(1 - \tau_{3i})}{2} \psi_i A_\mu. \end{aligned} \quad (7)$$

All the quantities have their usual well known meanings. From the relativistic Lagrangian we obtain the field equations for the nucleons and mesons. These equations are solved by expanding the upper and lower components of the Dirac spinors and the boson fields in an axially deformed harmonic oscillator basis with an initial deformation. The set of coupled equations is solved numerically by a self-consistent iteration method.

The centre-of-mass motion energy correction is estimated by the usual harmonic oscillator formula  $E_{c.m.} =$

$\frac{3}{4}(41A^{-1/3})$ . The constant gap BCS pairing is used to add the pairing effects for the open shell nuclei. It is to be noted that in the present work only intrinsic state solutions are presented. Each of these deformed intrinsic states is a superposition of various angular momenta states. To obtain the good angular momentum states and spectroscopic predictions for these nuclei near neutron drip-line we need to project out states of good angular momenta. Such calculation will be considered as a future extension of this work. The quadrupole moment deformation parameter  $\beta_2$  is evaluated from the resulting proton and neutron quadrupole moments, as  $Q = Q_n + Q_p = \sqrt{\frac{16\pi}{5}} (\frac{3}{4\pi} AR^2 \beta_2)$ . The root mean square (rms) matter radius is defined as  $\langle r_m^2 \rangle = \frac{1}{A} \int \rho(r_\perp, z) r^2 d\tau$ ; here  $A$  is the mass number, and  $\rho(r_\perp, z)$  is the deformed density. The total binding energy and other observables are also obtained by using the standard relations, given in [16]. We use the well known NL3 parameter set [18]. This set not only reproduces the properties of stable nuclei but also well predicts for those far from the  $\beta$ -stability valley. Also, the isoscalar monopole energy agrees excellently with the experimental values for different regions of the Periodic Table. The measured superdeformed minimum in  $^{194}\text{Hg}$  is 6.02 MeV above the ground state, whereas in RMF calculation with NL3 set, this number is 5.99 MeV [18]. All these facts give us confidence to use this older, though very much still in use, NL3 set for the present investigation.

## III. RESULTS AND DISCUSSION

### A. Ground state properties from the SHF and RMF models

There exists a number of parameter sets for the standard SHF and RMF Hamiltonians and Lagrangians. In some of our previous papers and of other authors [16, 18–21] the ground state properties, like the binding energies (BE), quadrupole moment deformation parameters  $\beta_2$ , charge radii ( $r_c$ ) and other bulk properties are evaluated by using the various non-relativistic and relativistic parameter sets. It is found that, more or less, most of the recent parameters reproduce well the ground state properties, not only of stable normal nuclei but also of exotic nuclei which are away from the valley of beta-stability. So, if one uses a reasonably acceptable parameter set the prediction of the results will remain nearly force independent. This is valid both for SHF and RMF formalisms. However, with a careful inspection of these parametrizations, some of the SHF and RMF sets can not reproduce the empirical data. In this context we can cite the deviation of isotopic shifts than the experimental data [22] for Pb nuclei while using SHF forces like, SkM\* values [23]. However, the RMF sets reproduce the kink quite nicely [24]. On the other hand, most of the RMF sets over estimate the nuclear matter incompressibility. In general, the predictive power of both the formalisms are reasonably well and can be comparable to each other, which can be seen in the subsequent subsections. In addition to this, the general results SHF (SkI4) and RMF (NL3) forces are similar for the considered region. Thus in the sub-

TABLE I: The calculated ground state binding energy obtained from SHF and RMF theory are compared with the experimentally known heaviest isotope for Ne, Na, Mg, Al, Si and S [25].

nucleus	RMF	SHF	Expt.	nucleus	RMF	SHF	Expt.
<sup>30</sup> Ne	215.1	210.6	211.2	<sup>33</sup> Na	237.9	234.5	232.8
<sup>34</sup> Mg	257.7	255.1	256.2	<sup>39</sup> Al	285.2	281.9	283.1
<sup>41</sup> Si	310.1	305.1	306.6	<sup>45</sup> S	353.5	350.2	354.2

TABLE II: The predicted neutron drip-line for Ne, Na, Mg, Al, Si and S in RMF (NL3) and SHF (SKI4) parameter sets are compared with prediction of infinite nuclear matter (INM) mass model [26], finite range droplet model (FRDM) [27] and experimental data [25] along with the number shown in parenthesis are the experimentally extrapolated values.

nucleus	RMF	SHF	INM	FRDM	Expt.
Ne	34	34	36	32	30 (34)
Na	40	37	40	36	33 (37)
Mg	40	40	46	40	34 (40)
Al	48	48	48	45	39 (42)
Si	54	48	50	48	41 (44)
S	55	55	53	50	45 (49)

sequent results during our discussion we will refer the results of RMF (NL3) calculations, except some specific cases. Thus the result of SHF (SKI4) are not displayed in Tables.

## B. Binding energy and neutron drip-line

The ground state binding energy (BE) are calculated for Ne, Na, Mg, Al, Si and S isotopes near the neutron drip-line. This is done by comparing the prolate, oblate and spherical solution of binding energy for a particular nucleus. For a given nucleus, the maximum binding energy corresponds to the ground state and other solutions are obtained as various excited intrinsic states. In Table I, the ground state binding energy for the heaviest isotopes for the nuclei discussed are compared with the experimental data [25]. From the Table it is observed that the calculated binding energies are comparable with SHF and RMF results. We have listed the neutron drip-lines in Table II, which are obtained from the ground state binding energy for neutron rich Ne, Na, Mg, Al, Si and S nuclei. The nuclei with the largest neutron numbers so far experimentally detected in an isotopic chain till date, known as experimental neutron drip-line are also displayed in this Table for comparison. The numbers given in the parenthesis are the experimentally extrapolated values[25]. To get a qualitative understanding of the prediction of neutron drip-line, we have compared our results with the infinite nuclear matter (INM) [26] and finite range droplet model (FRDM) [27] mass estimation. From the table, it is clear that all the predictions for neutron drip-line are comparable to each other.

The drip-lines are very important after discovery of the two isotopes <sup>40</sup>Mg and <sup>42</sup>Al [6] that here once predicted to be beyond the drip-line [7, 28]. This suggests that the drip-line is somewhere in the heavier side of the mass prediction which are beyond the scope of the present mass models [7, 28]. In

TABLE III: The calculated value of charge radius ( $r_{ch}$ ), quadrupole moment deformation parameter  $\beta_2$  and binding energy (BE) for Ne, Na and Mg nuclei in RMF (NL3) formalism. The maximum binding energy is the ground state solution and all other values are the intrinsic excited state solution. The radius  $r_{ch}$  is in fm and the binding energy is in MeV.

nucleus	$r_{ch}$	$\beta_2$	BE(MeV)	nucleus	$r_{ch}$	$\beta_2$	BE(MeV)
<sup>20</sup> Ne	2.970	0.535	156.7	<sup>20</sup> Ne	2.901	-0.244	152.0
<sup>21</sup> Ne	2.953	0.516	165.9	<sup>21</sup> Ne	2.889	-0.241	161.1
<sup>22</sup> Ne	2.940	0.502	175.7	<sup>22</sup> Ne	2.881	-0.242	170.5
<sup>23</sup> Ne	2.913	0.386	181.8	<sup>23</sup> Ne	2.880	-0.249	179.7
<sup>24</sup> Ne	2.890	0.278	188.9	<sup>24</sup> Ne	2.881	-0.259	188.9
<sup>25</sup> Ne	2.907	0.272	194.2	<sup>25</sup> Ne	2.886	-0.206	194.2
<sup>26</sup> Ne	2.926	0.277	199.9	<sup>26</sup> Ne	2.893	-0.159	199.9
<sup>27</sup> Ne	2.945	0.247	203.9	<sup>27</sup> Ne	2.925	-0.183	203.9
<sup>28</sup> Ne	2.965	0.225	208.2	<sup>28</sup> Ne	2.957	-0.203	208.2
<sup>29</sup> Ne	2.981	0.161	211.2	<sup>29</sup> Ne	2.974	-0.133	211.2
<sup>30</sup> Ne	2.998	0.100	215.0	<sup>30</sup> Ne	2.995	-0.081	215.0
<sup>31</sup> Ne	3.031	0.244	216.0	<sup>31</sup> Ne	3.013	-0.133	216.0
<sup>32</sup> Ne	3.071	0.373	218.6	<sup>32</sup> Ne	3.033	-0.180	218.6
<sup>33</sup> Ne	3.095	0.424	219.5	<sup>33</sup> Ne	3.044	-0.230	219.5
<sup>34</sup> Ne	3.119	0.473	220.9	<sup>34</sup> Ne	3.054	-0.275	220.9
<sup>35</sup> Ne	3.132	0.505	220.4	<sup>35</sup> Ne	3.064	-0.315	215.7
<sup>36</sup> Ne	3.146	0.539	220.3	<sup>36</sup> Ne	3.075	-0.352	220.4
<sup>24</sup> Na	2.939	-0.250	189.4	<sup>24</sup> Na	2.964	0.379	192.3
<sup>25</sup> Na	2.938	-0.258	200.3	<sup>25</sup> Na	2.937	0.273	200.6
<sup>26</sup> Na	2.940	-0.202	206.3	<sup>26</sup> Na	2.965	0.295	207.1
<sup>27</sup> Na	2.946	-0.157	212.5	<sup>27</sup> Na	2.993	0.323	214.2
<sup>28</sup> Na	2.980	-0.184	217.7	<sup>28</sup> Na	2.993	0.272	219.0
<sup>29</sup> Na	3.012	-0.205	223.4	<sup>29</sup> Na	3.004	0.232	224.3
<sup>30</sup> Na	3.025	-0.131	227.5	<sup>30</sup> Na	3.031	0.169	228.1
<sup>31</sup> Na	3.043	-0.074	232.5	<sup>31</sup> Na	3.047	0.108	232.7
<sup>32</sup> Na	3.061	-0.129	233.0	<sup>32</sup> Na	3.077	0.237	234.5
<sup>33</sup> Na	3.082	-0.179	234.3	<sup>33</sup> Na	3.113	0.356	237.9
<sup>34</sup> Na	3.095	-0.226	234.8	<sup>34</sup> Na	3.137	0.404	239.8
<sup>35</sup> Na	3.108	-0.270	235.9	<sup>35</sup> Na	3.161	0.450	242.3
<sup>36</sup> Na	3.121	-0.308	236.9	<sup>36</sup> Na	3.175	0.481	242.5
<sup>37</sup> Na	3.135	-0.345	238.4	<sup>37</sup> Na	3.190	0.512	243.1
<sup>38</sup> Na	3.156	-0.359	240.0	<sup>38</sup> Na	3.199	0.491	243.4
<sup>39</sup> Na	3.180	-0.375	241.8	<sup>39</sup> Na	3.209	0.472	244.1
<sup>40</sup> Na	3.184	-0.358	241.3	<sup>40</sup> Na	3.228	0.477	243.4
<sup>24</sup> Mg	3.043	0.487	194.3	<sup>24</sup> Mg	3.001	-0.256	186.8
<sup>25</sup> Mg	3.009	0.376	202.9	<sup>25</sup> Mg	2.993	-0.261	199.1
<sup>26</sup> Mg	2.978	0.273	212.5	<sup>26</sup> Mg	2.990	-0.268	211.6
<sup>27</sup> Mg	3.015	0.310	220.2	<sup>27</sup> Mg	2.988	-0.204	218.2
<sup>28</sup> Mg	3.048	0.345	228.7	<sup>28</sup> Mg	2.992	-0.154	225.6
<sup>29</sup> Mg	3.055	0.289	234.3	<sup>29</sup> Mg	3.027	-0.186	232.0
<sup>30</sup> Mg	3.062	0.241	240.5	<sup>30</sup> Mg	3.059	-0.207	239.0
<sup>30</sup> Mg	3.131	0.599	237.7				
<sup>31</sup> Mg	3.075	0.179	245.1	<sup>31</sup> Mg	3.068	-0.128	244.0
<sup>32</sup> Mg	3.090	0.119	250.5	<sup>32</sup> Mg	3.085	-0.067	249.9
<sup>32</sup> Mg	3.131	0.471	248.8				
<sup>33</sup> Mg	3.117	0.233	253.1	<sup>33</sup> Mg	3.102	-0.126	251.5
<sup>34</sup> Mg	3.150	0.343	257.3	<sup>34</sup> Mg	3.124	-0.181	253.9
<sup>34</sup> Mg	3.184	0.588	254.1				
<sup>35</sup> Mg	3.173	0.388	260.5	<sup>35</sup> Mg	3.141	-0.196	255.3
<sup>36</sup> Mg	3.198	0.432	263.9	<sup>36</sup> Mg	3.160	-0.213	257.0
<sup>37</sup> Mg	3.212	0.462	264.9	<sup>37</sup> Mg	3.179	-0.258	258.8
<sup>38</sup> Mg	3.227	0.492	266.3	<sup>38</sup> Mg	3.198	-0.300	261.1
<sup>39</sup> Mg	3.237	0.473	267.8	<sup>39</sup> Mg	3.216	-0.338	263.4
<sup>40</sup> Mg	3.247	0.456	269.7	<sup>40</sup> Mg	3.234	-0.374	266.4

TABLE IV: Same as Table III, but for Al, Si and S.

nucleus	$r_{ch}$	$\beta_2$	BE(MeV)	nucleus	$r_{ch}$	$\beta_2$	BE(MeV)
<sup>24</sup> Al	3.097	0.388	182.3	<sup>24</sup> Al	3.077	-0.258	179.4
<sup>25</sup> Al	3.072	0.381	197.7	<sup>25</sup> Al	3.060	-0.266	193.9
<sup>26</sup> Al	3.191	0.550	206.6	<sup>26</sup> Al	3.052	-0.275	207.8
<sup>27</sup> Al	3.215	0.572	217.0	<sup>27</sup> Al	3.053	-0.292	221.9
<sup>28</sup> Al	3.178	0.471	226.7	<sup>28</sup> Al	3.037	-0.208	238.6
<sup>29</sup> Al	3.061	0.251	239.3	<sup>29</sup> Al	3.033	-0.141	245.6
<sup>30</sup> Al	3.073	0.207	246.2	<sup>30</sup> Al	3.070	-0.184	253.8
<sup>31</sup> Al	3.085	0.170	253.6	<sup>31</sup> Al	3.101	-0.205	259.8
<sup>32</sup> Al	3.101	0.113	260.0	<sup>32</sup> Al	3.103	-0.111	261.2
<sup>33</sup> Al	3.118	0.057	267.2	<sup>33</sup> Al	3.165	-0.333	269.4
<sup>34</sup> Al	3.139	0.159	269.9	<sup>34</sup> Al	3.134	-0.108	275.1
<sup>35</sup> Al	3.167	0.268	274.1	<sup>35</sup> Al	3.157	-0.172	272.8
<sup>36</sup> Al	3.187	0.313	277.6	<sup>36</sup> Al	3.173	-0.189	277.7
<sup>37</sup> Al	3.208	0.355	281.5	<sup>37</sup> Al	3.191	-0.208	280.3
<sup>38</sup> Al	3.275	0.418	282.7	<sup>38</sup> Al	3.214	-0.254	283.5
<sup>39</sup> Al	3.285	0.406	285.1	<sup>39</sup> Al	3.236	-0.299	286.7
<sup>40</sup> Al	3.304	0.441	287.6	<sup>40</sup> Al	3.257	-0.336	290.4
<sup>41</sup> Al	3.325	0.474	290.5	<sup>41</sup> Al	3.278	-0.370	290.6
<sup>42</sup> Al	3.348	0.483	290.7	<sup>42</sup> Al	3.281	-0.355	291.2
<sup>43</sup> Al	3.371	0.491	291.3	<sup>43</sup> Al	3.282	-0.338	292.2
<sup>44</sup> Al	3.375	0.456	291.0	<sup>44</sup> Al	3.274	-0.288	293.6
<sup>45</sup> Al	3.378	0.420	291.0	<sup>45</sup> Al	3.271	-0.263	293.5
<sup>46</sup> Al	3.359	0.341	294.5	<sup>46</sup> Al	3.346	-0.296	294.0
<sup>46</sup> Al	3.246	0.125	293.6	<sup>46</sup> Al	3.432	0.660	290.8
<sup>47</sup> Al	3.246	0.090	294.8	<sup>47</sup> Al	3.335	-0.319	293.6
<sup>47</sup> Al	3.447	0.653	290.4				
<sup>48</sup> Al	3.276	0.117	293.8	<sup>48</sup> Al	3.319	-0.252	294.0
<sup>24</sup> Si	3.162	0.294	169.1	<sup>24</sup> Si	3.170	-0.278	169.3
<sup>25</sup> Si	3.127	0.286	185.1	<sup>25</sup> Si	3.139	-0.274	184.8
<sup>26</sup> Si	3.099	0.282	201.8	<sup>26</sup> Si	3.118	-0.280	200.9
<sup>27</sup> Si	3.054	0.168	215.8	<sup>27</sup> Si	3.114	-0.299	216.4
<sup>28</sup> Si	3.017	0.001	231.4	<sup>28</sup> Si	3.122	-0.331	232.1
<sup>29</sup> Si	3.035	0.001	240.7	<sup>29</sup> Si	3.093	-0.237	240.7
<sup>30</sup> Si	3.070	0.148	250.6	<sup>30</sup> Si	3.054	-0.060	250.4
<sup>31</sup> Si	3.089	0.120	258.7	<sup>31</sup> Si	3.108	-0.180	259.1
<sup>32</sup> Si	3.109	0.104	267.2	<sup>32</sup> Si	3.137	-0.201	268.5
<sup>33</sup> Si	3.126	0.050	275.4	<sup>33</sup> Si	3.131	-0.084	275.6
<sup>34</sup> Si	3.148	0.000	284.4	<sup>34</sup> Si	3.204	-0.336	278.5
<sup>35</sup> Si	3.160	0.085	287.3	<sup>35</sup> Si	3.161	-0.083	287.4
<sup>36</sup> Si	3.184	0.193	291.4	<sup>36</sup> Si	3.186	-0.162	291.5
<sup>37</sup> Si	3.200	0.238	295.4	<sup>37</sup> Si	3.201	-0.181	294.8
<sup>38</sup> Si	3.218	0.281	299.8	<sup>38</sup> Si	3.219	-0.204	298.8
<sup>39</sup> Si	3.224	0.263	302.4	<sup>39</sup> Si	3.245	-0.254	301.9
<sup>40</sup> Si	3.232	0.244	305.4	<sup>40</sup> Si	3.272	-0.301	306.0
<sup>41</sup> Si	3.230	0.167	307.1	<sup>41</sup> Si	3.295	-0.336	310.1
<sup>42</sup> Si	3.228	0.013	309.8	<sup>42</sup> Si	3.318	-0.369	314.6
<sup>43</sup> Si	3.240	0.123	311.8	<sup>43</sup> Si	3.320	-0.356	315.2
<sup>44</sup> Si	3.252	0.172	314.3	<sup>44</sup> Si	3.322	-0.342	316.2
<sup>45</sup> Si	3.252	0.117	315.8	<sup>45</sup> Si	3.316	-0.308	317.5
<sup>46</sup> Si	3.253	0.053	317.9	<sup>46</sup> Si	3.303	-0.262	319.3
<sup>47</sup> Si	3.258	0.005	319.7	<sup>47</sup> Si	3.345	-0.298	319.8
<sup>48</sup> Si	3.263	0.001	321.8	<sup>48</sup> Si	3.381	-0.321	320.8
<sup>49</sup> Si	3.290	0.045	321.1	<sup>49</sup> Si	3.366	-0.251	320.7
<sup>50</sup> Si	3.319	0.074	321.1	<sup>50</sup> Si	3.341	-0.159	321.5
<sup>51</sup> Si	3.345	0.078	321.1	<sup>51</sup> Si	3.358	-0.135	321.2
<sup>52</sup> Si	3.371	0.082	321.4	<sup>52</sup> Si	3.377	-0.112	321.2
<sup>53</sup> Si	3.391	0.042	321.6	<sup>53</sup> Si	3.391	-0.052	321.3
<sup>54</sup> Si	3.415	0.000	322.3	<sup>54</sup> Si	3.415	-0.010	322.0

TABLE V: Same as Table III, but for S.

nucleus	$r_{ch}$	$\beta_2$	BE(MeV)	nucleus	$r_{ch}$	$\beta_2$	BE(MeV)
<sup>33</sup> S	3.241	0.197	275.5	<sup>33</sup> S	3.233	-0.116	275.1
<sup>34</sup> S	3.248	0.140	285.8	<sup>34</sup> S	3.257	-0.168	286.5
<sup>35</sup> S	3.260	0.077	295.6	<sup>35</sup> S	3.260	-0.078	295.7
<sup>36</sup> S	3.273	0.002	306.2	<sup>36</sup> S	3.309	-0.308	299.7
<sup>37</sup> S	3.285	0.152	311.6	<sup>37</sup> S	3.287	-0.116	310.1
<sup>38</sup> S	3.300	0.228	318.6	<sup>38</sup> S	3.300	-0.164	316.9
<sup>39</sup> S	3.312	0.264	325.3	<sup>39</sup> S	3.307	-0.173	322.6
<sup>40</sup> S	3.325	0.299	332.4	<sup>40</sup> S	3.316	-0.181	328.5
<sup>41</sup> S	3.331	0.287	337.7	<sup>41</sup> S	3.324	-0.189	333.6
<sup>42</sup> S	3.338	0.277	343.2	<sup>42</sup> S	3.335	-0.207	339.2
<sup>43</sup> S	3.359	0.318	347.2	<sup>43</sup> S	3.348	-0.229	344.1
<sup>44</sup> S	3.381	0.367	351.0	<sup>44</sup> S	3.366	-0.263	349.5
<sup>45</sup> S	3.375	0.312	353.4	<sup>45</sup> S	3.367	-0.240	351.8
<sup>46</sup> S	3.371	0.258	356.6	<sup>46</sup> S	3.375	-0.237	355.1
<sup>47</sup> S	3.385	0.257	358.5	<sup>47</sup> S	3.380	-0.230	358.0
<sup>48</sup> S	3.400	0.259	360.8	<sup>48</sup> S	3.389	-0.230	360.8
<sup>49</sup> S	3.403	0.227	362.9	<sup>49</sup> S	3.420	-0.257	362.9
<sup>50</sup> S	3.403	0.189	365.5	<sup>50</sup> S	3.451	-0.277	365.0
<sup>51</sup> S	3.427	0.188	366.4	<sup>51</sup> S	3.451	-0.231	365.9
<sup>52</sup> S	3.451	0.183	367.6	<sup>52</sup> S	3.447	-0.178	367.6
<sup>53</sup> S	3.463	0.158	369.1	<sup>53</sup> S	3.466	-0.172	368.4
<sup>54</sup> S	3.477	0.139	371.0	<sup>54</sup> S	3.486	-0.142	369.8
<sup>55</sup> S	3.494	0.105	371.4	<sup>55</sup> S	3.497	-0.090	370.5

this calculations the newly discovered nuclei <sup>40</sup>Mg and <sup>42</sup>Al are well within the prediction both in the SHF and RMF formalisms. Again a further comparison of the drip-line with RMF and SHF prediction, we find the drip-line predictions in both calculations are well comparable, except for a few exceptions in Na and Si as shown in Table II.

### C. Neutron configuration

Analysing the neutron configuration for these exotic nuclei, we notice that, for lighter isotopes of Ne, Na, Mg, Al, Si and S the oscillator shell  $N_{osc} = 3$  is empty. However, the  $N_{osc} = 3$  shell gets occupied gradually with increase of neutron number. In case of Na,  $N_{osc} = 3$  starts filling up at <sup>33</sup>Na with quadrupole moment deformation parameter  $\beta_2 = 0.356$  and  $-0.179$  with occupied orbits  $[330]1/2^-$  and  $[303]7/2^-$ , respectively. The filling of  $N_{osc} = 3$  goes on increasing for Na with neutron number and it is  $[330]1/2^-$ ,  $[310]1/2^-$ ,  $[321]3/2^-$  and  $[312]5/2^-$  at  $\beta_2 = 0.472$  for <sup>39</sup>Na. Again for the oblate solution the occupation is  $[301]1/2^-$ ,  $[301]3/2^-$ ,  $[303]5/2^-$  and  $[303]7/2^-$  for  $\beta_2 = -0.375$  for <sup>39</sup>Na. In the case of Mg isotopes, even for <sup>30,32</sup>Mg, the  $N_{osc} = 3$  shell have some occupation for the low-lying excited states near the Fermi surface for <sup>30</sup>Mg (at  $\beta = 0.599$  with  $BE = 237.721$  MeV the  $N_{osc}=3$  orbit is  $[330]7/2^-$  and for <sup>32</sup>Mg:  $\beta_2 = [330]1/2^-$ ,  $BE=248.804$  MeV at  $\beta_2 = 0.471$ ). With the increase of neutron number in Mg and Si isotopic chain, the oscillator shell with  $N_{osc} = 3$  gets occupied more and more. For most of the Si isotopes, the oblate solutions are the dominating ones than the low-lying prolate superdeformed states,

TABLE VI: The calculated value of charge radii ( $r_{ch}$ ), quadrupole deformation parameter  $\beta_2$  and binding energy (BE) for Ne, Mg, Si and S even-even nuclei in SHF (SkI4) formalism. The maximum binding energy is the ground state solution and all other values are the intrinsic excited state solution. The radius  $r_{ch}$  is in fm and the binding energy is in MeV.

nucleus	$r_{ch}$	$\beta_2$	BE(MeV)	$r_{ch}$	$\beta_2$	BE(MeV)
<sup>20</sup> Ne	3.029	0.5481	156.817	2.950	-0.1356	154.474
<sup>22</sup> Ne	3.005	0.5223	175.758	2.943	-0.1989	172.758
<sup>24</sup> Ne	2.952	0.2546	188.354	2.951	-0.2541	188.538
<sup>26</sup> Ne	2.953	0.1233	199.380	2.944	0.0060	199.389
<sup>28</sup> Ne	3.013	0.1623	206.524	3.010	-0.1334	206.433
<sup>30</sup> Ne	3.054	0.0030	213.721			
<sup>32</sup> Ne	3.103	0.3808	213.118	3.118	0.3716	213.215
<sup>34</sup> Ne	3.179	0.4880	213.483	3.108	-0.1462	209.695
<sup>36</sup> Ne	3.203	0.6015	212.230	3.147	-0.2789	208.770
<sup>24</sup> Mg	3.128	0.5248	195.174	3.077	-0.252	189.946
<sup>26</sup> Mg	3.090	0.3623	212.885	3.079	-0.2988	213.153
<sup>28</sup> Mg	3.111	0.3419	228.997	3.056	-0.1076	227.899
<sup>30</sup> Mg	3.119	0.2022	240.328	3.117	-0.1835	240.514
<sup>32</sup> Mg	3.145	0.0000	252.033	3.145	0.0000	252.033
<sup>34</sup> Mg	3.209	0.3263	255.067	3.175	-0.1196	253.455
<sup>35</sup> Mg	3.295	0.4884	201.512	3.252	-0.289	257.634
<sup>36</sup> Mg	3.265	0.4413	259.899	3.213	-0.2124	255.368
<sup>40</sup> Mg	3.321	0.4741	262.796	3.299	-0.3538	260.200
<sup>28</sup> Si	3.117	0.009	231.037	3.194	-0.3494	233.590
<sup>30</sup> Si	3.145	0.1477	252.146	3.168	-0.2102	252.625
<sup>32</sup> Si	3.179	0.007	269.479	3.199	-0.1990	270.483
<sup>34</sup> Si	3.216	0.000	286.332			
<sup>36</sup> Si	3.146	0.1549	292.418	3.241	-0.009	292.425
<sup>38</sup> Si	3.291	0.3051	298.173	3.279	-0.1978	298.173
<sup>40</sup> Si	3.325	0.2990	230.450	3.309	-0.2817	303.969
<sup>42</sup> Si	3.349	0.3592	307.399	3.334	-0.3508	310.023
<sup>44</sup> Si	3.334	0.2119	309.712	3.377	-0.3031	311.601
<sup>46</sup> Si	3.337	0.009	312.451	3.372	-0.2405	313.508
<sup>48</sup> Si	3.348	0.002	315.425	3.438	-0.2893	313.995
<sup>30</sup> S	3.262	0.1491	241.434	3.178	-0.1856	241.385
<sup>32</sup> S	3.271	0.200	208.173	3.256	-0.1700	267.975
<sup>34</sup> S	3.288	0.1212	288.804	3.295	-0.1566	289.304
<sup>36</sup> S				3.314	-0.003	309.619
<sup>38</sup> S	3.341	0.2144	320.168	3.331	-0.1289	318.951
<sup>40</sup> S	3.374	0.3042	332.097	3.350	-0.1529	327.809
<sup>42</sup> S	3.392	0.2898	341.033	3.379	-0.2195	337.031
<sup>44</sup> S	3.436	0.3677	348.266	3.410	-0.2714	346.445
<sup>46</sup> S	3.423	0.2517	352.486	3.413	-0.2090	351.578
<sup>48</sup> S	3.450	0.2379	356.188	3.430	-0.2032	356.589
<sup>50</sup> S	3.441	0.1229	360.815	3.498	-0.2673	359.011
<sup>52</sup> S	3.482	0.1099	362.347	3.487	-0.1356	362.531
<sup>54</sup> S	3.528	0.003	364.650	3.524	-0.1023	363.926
<sup>56</sup> S	3.558	0.1105	366.031	3.556	-0.0100	366.033

i.e. mass of the oblate solutions are the ground state solutions and the prolate and some superdeformed are the excited configurations. Again, in S-isotopes, the prolate are the ground state and the oblate are the extreme excited states. Note that in many cases, there exist low laying superdeformed states and some of them are listed in the Tables.

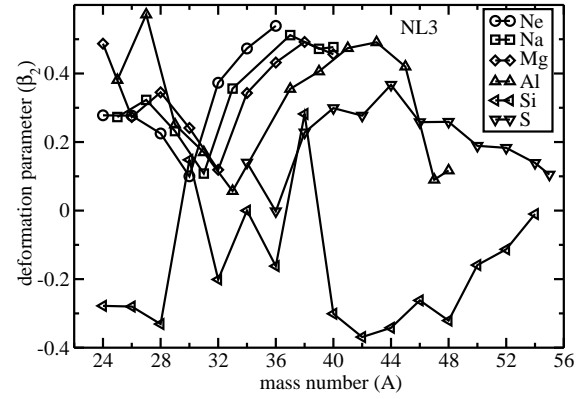


FIG. 1: The ground state quadrupole deformation parameter  $\beta_2$  versus mass number  $A$  for Ne, Na, Mg, Al, Si and S isotopes near the drip-line with NL3 parameter set.

#### D. Quadrupole deformation

The ground and low-lying excited state deformation systematics for some of the representative nuclei for Ne, Na, Mg, Al, Si and S are analysed. In Fig. 1, the ground state quadrupole deformation parameter  $\beta_2$  is shown as a function of mass number for Ne, Na, Mg, Al, Si and S. The  $\beta_2$  value goes on increasing with mass number for Ne, Na and Mg isotopes near the drip-line. The calculated quadrupole deformation parameter  $\beta_2$  for <sup>34</sup>Mg is 0.59 which compares well with the recent experimental measurement of Iwasaki et al [3] ( $\beta_2 = 0.58 \pm 6$ ). Note that this superdeformed states in 3.2 MeV above than the ground band. Again, the magnitude of  $\beta_2$  for the drip-line nuclei reduces with neutron number  $N$  and again increases. A region of maximum deformation is found for almost all the nuclei as shown in the figure. It so happens in cases like, Ne, Na, Mg and Al that the isotopes are maximum deformed which may be comparabled to superdeformed near the drip-line. For Si isotopes, in general, we find oblate solution in the ground configurations. In many of the cases, the low-lying superdeformed configuration are clearly visible and some of them are available in the Tables.

#### E. Shape coexistence

One of the most interesting phenomena in nuclear structure physics is the shape coexistence [29–31]. In many of the cases for the nuclei considered here near the drip-line isotopes, the ground state configuration accompanies a low-lying excited state. In few cases, it so happens that these two solutions are almost degenerate. That means we predict almost similar binding energy for two different configurations. For example, in the RMF calculation, the ground state binding energy of <sup>24</sup>Ne is 189.093 MeV with  $\beta_2 = -0.259$  and the binding energy of the excited low-lying configuration at  $\beta_2 = 0.278$  is 188.914 MeV. The difference in BE of these two solutions is only 0.179 MeV. Similarly the solution of prolate-oblate binding energy difference in SkI4 is 0.186 MeV for <sup>30</sup>Mg with

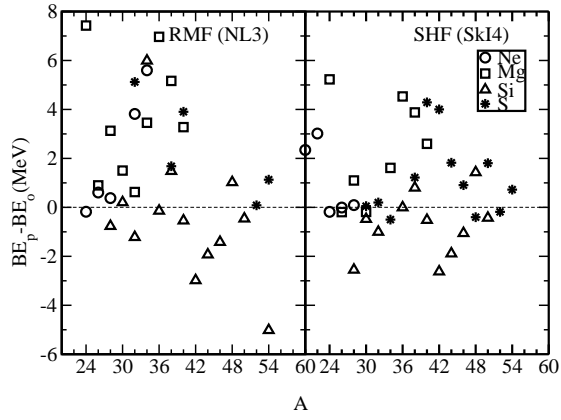


FIG. 2: The difference in binding energy between the prolate-oblate solutions is shown for even-even Ne, Mg, Si and S isotopes near the neu

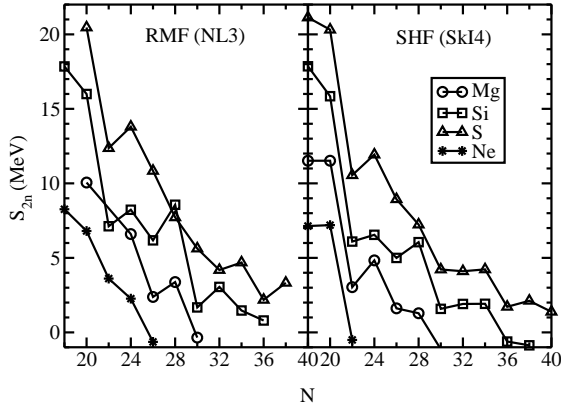


FIG. 3: The two-neutron separation  $S_{2n}$  energy versus neutron number  $N$  for neutron-rich Ne, Mg, Si and S isotopes.

$\beta_2 = -0.183$  and  $0.202$ . This phenomenon is clearly available in most of the isotopes near the drip-line. To show it in a more quantitative way, we have plotted the prolate-oblate binding energy difference in Figure 2. The left hand side of the figure is for relativistic and the right side is the nonrelativistic SkI4 results. From the figure, it is clear that an island of shape coexistence isotopes are available for Mg and Si isotopes. These shape coexistence solutions are predicted taking into account the intrinsic binding energy. However the actual quantitative energy difference of ground and excited configuration can be given by performing the angular momentum projection, which is be an interesting problem for future.

### F. Two neutron separation energy and new magic number

The appearance of new and the disappearance of known magic number near the neutron drip-line is a well discussed topic currently in nuclear structure physics [5, 32]. Some of the calculations in recent past predicted the disappearance of the known magic number  $N=28$  for the drip-line isotopes of Mg and S [33, 34]. However, magic number 20 retains its

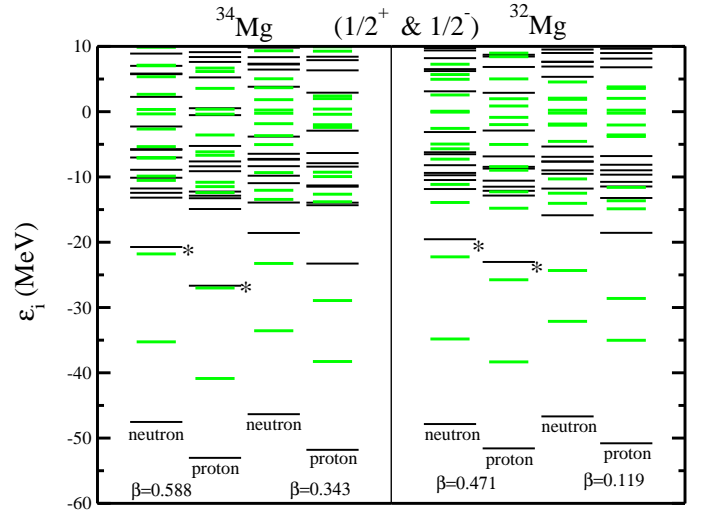


FIG. 4: The  $1/2^+$  and  $1/2^-$  intrinsic single-particle states for the normal and superdeformed state for  $^{32}\text{Mg}$  and  $^{34}\text{Mg}$ . A few of the lowest energy parity-doublet states of the superdeformed (SD) solutions are shown by asterisk for the SD configuration. More such doublets are noticed for the SD intrinsic states. The  $\pm 1/2^-$  states are denoted by shorter (and green) lines and the  $\pm 1/2^+$  states are denoted by longer (and black).

magic properties even for the drip-line region. In one of our earlier publications, [35] we analysed the spherical shell gap at  $N=28$  in  $^{44}\text{S}$  and its neighboring  $^{40}\text{Mg}$  and  $^{42}\text{Si}$  using NL-SH [22] and TM2 parameter sets [36]. The spherical shell gap at  $N=28$  in  $^{44}\text{S}$  was found to be intact for the TM2 and is broken for NL-SH parametrization. Here, we plot the two-neutron separation energy  $S_{2n}$  of Ne, Mg, Si and S for the even-even nuclei near the drip-line (fig 3). The known magic number  $N=28$  is noticed to be absent in  $^{44}\text{S}$ . On the other hand the appearance of steep  $2n$ -separation energy at  $N=34$  both in RMF and SHF calculation looks quite prominent, and this is just two units ahead than the experimental shell closure  $N=32$  [37].

### G. Superdeformation and Low $\Omega$ parity doublets

The deformation-driving  $m = 1/2^-$ -orbits come down in energy in superdeformed solutions from the shell above, in contrast to the normal deformed solutions. The occurrence of approximate  $1/2^+ 1/2^-$  parity doublets (degeneracy of  $|m|^\pi = 1/2^+ 1/2^-$  states) for the superdeformed solutions are clearly seen in Figs. 4 and 5 where excited superdeformed configurations for  $^{32}\text{Mg}$  and  $^{34}\text{Mg}$  and for  $^{46}\text{Al}$  and  $^{47}\text{Al}$  are given. For each nucleus we have compared the normal deformed ( $\beta_2 \sim 0.1 - 0.3$ ) and the superdeformed configurations and analysed the deformed orbits.

The  $1/2^+$  and  $1/2^-$  states for the single particle levels are shown in Fig. 4 (for  $^{32}\text{Mg}$  and  $^{34}\text{Mg}$ ). From the analysis of the results of this calculation, we have found a systematic behaviour of the low  $\Omega$  (particularly  $1/2^+$  and  $1/2^-$ ) prolate deformed orbits for the superdeformed solutions. As repre-

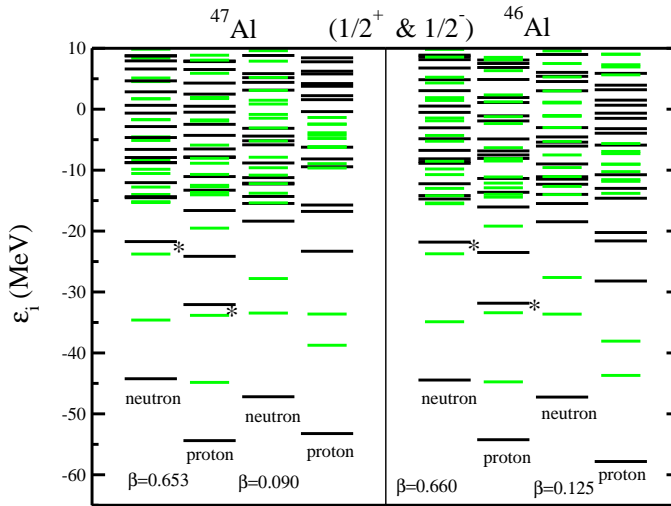


FIG. 5: Same as Fig. 4 for  $^{46}\text{Al}$  and  $^{47}\text{Al}$ .

sensitive cases, we present here results for ( $^{34}\text{Mg} - ^{32}\text{Mg}$ ) and ( $^{47}\text{Al} - ^{46}\text{Al}$ ) and plot the  $1/2^+$  and  $1/2^-$  orbits for the superdeformed and normal deformed shapes of these nuclei. We notice from the plot of the orbits that there is occurrence of  $1/2^+$  and  $1/2^-$  orbits very closely in energy for the superdeformed (SD) shape. Two such  $1/2^+$  and  $1/2^-$  doublet structures, marked in asterisk are shown in Figs. 4 and 5 for the SD solutions. Such  $1/2^+$   $1/2^-$  degenerate orbits occur not only for the well-bound orbits but also for the unbound continuum states. As example, the doublet neutrons  $[220]1/2^+$  and  $[101]1/2^-$  states is 4 MeV apart in energy in the normal deformed prolate solutions tend to become degenerate in the SD solution  $[220]1/2^+$  and  $[101]1/2^-$  states (prolate) belonging to two different major shells, so close to each other in the superdeformed solution (shown in Figs. 4 for  $^{34}\text{Mg}$ ). More such doublets are easily identified (Figs. 4 and 5) for superdeformed solutions of  $^{32,34}\text{Mg}$  and  $^{46,47}\text{Al}$ . In fact it is noticed that the  $\Omega = 1/2$  states of unique parity, seen clearly well separated in the normal deformed solutions, get quite close to each other for the SD states, suggesting degenerate parity doublet structure. This can lead to parity mixing and octupole deformed shapes for the SD structures [38]. Parity doublets and octupole deformation for superdeformed solutions have been

discussed for neutron-rich Ba and Zr nuclei [39]. There is much interest for the experimental study of the spectra of neutron-rich nuclei in this mass region [40]. The highly deformed structures for the neutron-rich  $Ne - Na - Mg - Al$  nuclei are interesting and signature of such superdeformed configurations should be looked for.

#### IV. SUMMARY AND CONCLUSION

In summary, we calculate the ground and low-lying excited state properties, like binding energy and quadrupole deformation  $\beta_2$  using NL3 parameter set for Ne, Na, Mg, Si and S isotopes, near the neutron drip-line region. In general, we find large deformed solutions for the neutron-drip nuclei which agree well with the experimental measurement. We have done the calculation using the nonrelativistic Hartree-Fock formalism with Skyrme interaction SkI4. Both the relativistic and non-relativistic results were found comparable to each other for the considered mass region. In the present calculations a large number of low-lying intrinsic superdeformed excited states are observed for many of the isotopes and some of them are reported. The breaking of N=28 magic number and the appearance of a new magic number at N=34 appears in our calculations. A proper angular momentum projection may tell us the exact lowering of binding energy and it may happen that the superdeformed would be the ground band of some of the neutron-rich nuclei. Work in this direction is worth doing because of the present interest in the topic of the drip-line nuclei. In this study we find that, for the SD shape, the low  $\Omega$  orbits (particularly  $\Omega = 1/2$ ) become more bound and show a parity doublet structure. Closelying parity-doublet band structures and enhanced electromagnetic transition rates are a clear possibility for the superdeformed shapes.

#### V. ACKNOWLEDGMENTS

This work has been supported in part by Council of Scientific & Industrial Research (No. 03(1060)06/EMR-II) as well as projects No. SR/S2/HEP-16/2005 and SR/S2/HEP-037/2008, Department of Science and Technology, Govt. of India.

- 
- [1] A. Navin et al., Phys. Rev. Lett. **85** 266 (2000); H. Iwasaki et al., **B491**, 8 (2000); H. Iwasaki et al., **B481** 7 (2000).  
[2] T. Motobayashi et al., Phys. Lett. **B346** 9 (1995).  
[3] H. Iwasaki et al., **B522** 227 (2001).  
[4] S. K. Patra and C. R. Praharaaj, Phys. Lett. **B273** 13 (1991); Phys. Rev. **C47** 2978 (1993); Nucl. Phys. **A565** 442 (1993).  
[5] A. Ozawa, T. Kobayashi, T. Suzuki, K. Yoshida and I. Tanihata, Phys. Rev. Lett. **84** 5493 (2000).  
[6] T. Baumann et al., Nature **449** 1022 (2007).  
[7] P. Möller, R.J. Nix, W.D. Myers and W.J. Swiatecki, At. Data Nucl. Data Tables **59** 185 (1995).  
[8] D. Vautherin and D.M. Brink, Phys. Rev C **5** 626 (1972).  
[9] P.G. Reinhard, Rep. Prog. Phys. **52** 439 (1989).  
[10] E. Chabanat, P. Bonche, P. Hansel, J. Meyer, and R. Schaeffer, Nucl. Phys. A **627** 710 (1997).  
[11] J.R. Stone and P.-G. Reinhard, Prog. Part. Nucl. Phys. **58** 587 (2007).  
[12] J.R. Stone, J.C. Miller, R. Konciewicz, P.D. Stevenson, and M.R. Strayer, Phys. Rev. C **68** 034324 (2003).  
[13] P.-G. Reinhard and H. Flocard, Nucl. Phys. A **584**, 467 (1995).  
[14] E. Chabanat, P. Bonche, P. Haensel, J. Meyer, and R. Schaeffer, Nucl. Phys. **A635** 231 (1998).  
[15] B.D. Serot and J.D. Walecka, Adv. Nucl. Phys. **16** 1 (1986).  
[16] Y.K. Gambhir, P. Ring, and A. Thimet, Ann. Phys. (N.Y.) **198**

- 132 (1990).
- [17] B.A. Brown, Phys. Rev. **C58** 220 (1998).
- [18] G.A. Lalazissis, J. König, and P. Ring, Phys. Rev. **C55** 540 (1997).
- [19] P. Arumugam, B.K. Sharma, S.K. Patra, and R.K. Gupta, Phys. Rev. C **71** 064308 (2005).
- [20] S.K. Patra, C.-L. Wu, C.R. Praharaaj, and R.K. Gupta, Nucl. Phys. **A651** 117 (1999).
- [21] S.K. Patra, R.K. Gupta, B.K. Sharma, P.D. Stevenson, and W. Greiner, J. Phys. **G34** 2073 (2007).
- [22] M.M. Sharma, M.A. Nagarajan and P. Ring, Phys. Lett. **B312** 377 (1993).
- [23] N. Tajima, P. Bonchc, H. Flocard, P.-H. Heenen and M.S. Weiss, Nucl. Phys. **A551** 434 (1993).
- [24] M.M. Sharma, G.A. Lalazissis and P. Ring, Phys. Lett. **B317** 9 (1993).
- [25] G. Audi, A.H. Wapstra, and C. Thibault, Nucl. Phys. **A729** 337 (2003).
- [26] R.C. Nayak and L. Satpathy, At. Data and Nucl. Data Tables, **73** 213 (1999).
- [27] P. Möller, J. R. Nix and K. -L. Kratz, At. Data and Nucl. Data Tables, **66** 131 (1997).
- [28] M. Samyn, S. Goriely, M. Bender and J.M. Pearson, Phys. Rev. **C70** 044309 (2004).
- [29] J.P. Maharana, Y.K. Gambhir, J.A. Sheikh and P. Ring, Phys. Rev. **C46** R1163 (1992); S.K. Patra and C.R. Praharaaj, Phys. Rev. **C47** 2978 (1993).
- [30] F. Sarazin et al, Phys. Rev. Lett. **84** 5062 (2000).
- [31] J.L. Egido, L.M. Robledo, R.R. Rodriguez-Guzman, Phys. Rev. Lett. **93** 282502 (2004).
- [32] T.K. Jha, M.S. Mehta, S.K. Patra, B.K. Raj and Raj K. Gupta, PRAMANA -J. Phys. **61** 517 (2003); L. Satpathy and S.K. Patra, Nucl. Phys. **A722** 24c (2003); R.K. Gupta, M. Balasubramaniam, Sushil Kumar, S.K. Patra, G. Münzenberg and W. Greiner, J. Phys. **G32** 565 (2006); Raj K. Gupta, S. K. Patra and W. Greiner, Mod. Phys. Lett. **A12** 1327 (1997).
- [33] T.R. Werner, J.A. Sheikh, W. Nazarewicz, M.R. Strayer, A.S. Umar and M. Misu, Phys. Lett. **B335** 259 (1994).
- [34] Zhongzhou Ren, Z.Y. Zhub, Y.H. Cai and Gongou Xu, Phys. Lett. **B380** 241 (1994).
- [35] R. K. Gupta, S. K. Patra and W. Greiner, Mod. Phys. Lett. **A12** 1317 (1997).
- [36] Y. Sugahara and H. Toki, Nucl. Phys. **A579** 557 (1994).
- [37] R. Kanungo, I. Tanihata and A. Ozawa, Phys. Lett. **B528** 58 (2002).
- [38] C.R. Praharaaj, *INT Workshop on "Nuclear Many-Body Theories for 21st Century"*, University of Washington, Seattle (2007).
- [39] C.R. Praharaaj, *Structure of Atomic Nuclei*, Ch. 4, page 108, Edited by L. Satpathy; C.R. Praharaaj, J. Phys. **G12** L139 (1986).
- [40] D. Miller et al, Phys. Rev. **C79** 054306 (2009).